Unclassified

SECURITY CLASSIFICATION OF THIS PAGE

(2)

REPORT DOCUMENTATION PAGE

DTIC FILE COPY

1a. REPORT SECURITY CLASSIFICATION Unclassified	1b. RESTRICTIVE MARKINGS
2a. SECURITY CLASSIFICATION AUTHORITY	3. DISTRIBUTION/AVAILABILITY OF REPORT Approved for Public Release; Distribution Unlimited
2b. DECLASSIFICATION/DOWNGRADING SCHEDULE	
4. PERFORMING ORGANIZATION REPORT NUMBER(S) AFGL-TR-88-0289	5. MONITORING ORGANIZATION REPORT NUMBER(S)
6a. NAME OF PERFORMING ORGANIZATION Air Force Geophysics Laboratory 6b. OFFICE SYMBOL (If applicable) PHG	7a. NAME OF MONITORING ORGANIZATION
6c. ADDRESS (City, State, and ZIP Code) Hanscom AFB Massachusetts 01731-5000	7b. ADDRESS (City, State, and ZIP Code)
8a. NAME OF FUNDING/SPONSORING ORGANIZATION 8b. OFFICE SYMBOL (If applicable)	9. PROCUREMENT INSTRUMENT IDENTIFICATION NUMBER
8c. ADDRESS (City, State, and ZIP Code)	10. SOURCE OF FUNDING NUMBERS PROGRAM ELEMENT NO. 61102F; PROJECT NO. 2311; TASK NO. G5; WORK UNIT ACCESSION NO. 01

11. TITLE (Include Security Classification)
Average Low-Latitude Meridional Electric Fields From DE 2 During Solar Maximum

12. PERSONAL AUTHOR(S)
N.C. Maynard, T.L. Aggson, *F.A. Herrero*, M.C. Liebrecht#

13a. TYPE OF REPORT	13b. TIME COVERED	14. DATE OF REPORT (Year, Month, Day)	15. PAGE COUNT
Reprint	FROM _____ TO _____	1988 October 7	17

16. SUPPLEMENTARY NOTATION
*NASA Goddard Space Flight Center, Greenbelt Maryland, #Science Applications Research Inc., Lanham, Maryland - Reprinted from Journal of Geophysical Research Vol. 93, No. A5, Pages 4021-4037, May 1, 1988

17. COSATI CODES		
FIELD	GROUP	SUB-GROUP

18. SUBJECT TERMS (Continue on reverse if necessary and identify by block number)
Electric fields, Equatorial electrodynamics, Ionospheric convection

19. ABSTRACT (Continue on reverse if necessary and identify by block number)

Electric field data from the double probe vector electric field instrument (VEFI) on the DE 2 spacecraft have been analyzed to determine the average meridional electric field (zonal ion flow) patterns in the region between ± 30° magnetic latitude during solar maximum conditions. Over 300 passes were used to compile the data set. Data were projected to a constant 300-km altitude and to the equatorial plane assuming that the electric field along the magnetic field was zero. The average data set displayed a rapid increase of the downward meridional electric field with local time near 1800 MLT with the higher latitudes seeing the change first. A secondary nighttime maximum of this electric field component was observed post midnight with the crossover to upward electric fields (westward ion flow) occurring between 0400 and 0500 MLT. A sharp return to near zero was observed between 1200 and 1300. Typical average amplitudes range between 3 and 6 mV/m. No consistent variations with magnetic activity were observed. Although the daily variation in the zonal ion flow is dominated by the diurnal term, a net superrotation is evident in the harmonic analysis. The superrotation is strongest near the equator and decreases with latitude, because of the disturbance dynamo. The higher order harmonics up through the quatrediurnal term are also of significant magnitude in the analysis of the shape of the daily variation. Close similarity is seen to the zonal neutral winds indicating that they form the principal driving force. The magnitudes of the electric field derived ion drift are somewhat higher than the average F region neutral wind values. This along with the higher order harmonic content argues for the need to develop fully coupled E and F region model depicting the ionosphere and thermosphere interactions in a self-consistent fashion.

DTIC ELECTE OCT 14 1988 S E

20. DISTRIBUTION/AVAILABILITY OF ABSTRACT
☐ UNCLASSIFIED/UNLIMITED ☒ SAME AS RPT ☐ DTIC USERS

21. ABSTRACT SECURITY CLASSIFICATION
Unclassified

22a. NAME OF RESPONSIBLE INDIVIDUAL	22b. TELEPHONE (Include Area Code)	22c. OFFICE SYMBOL
N.C. Maynard	(617) 377-2431	PHG

DD FORM 1473, 84 MAR 83 APR edition may be used until exhausted. All other editions are obsolete.

SECURITY CLASSIFICATION OF THIS PAGE

AD-A200 338

JOURNAL OF GEOPHYSICAL RESEARCH, VOL. 93, NO. A5, PAGES 4021–4037, MAY 1, 1988

Average Low-Latitude Meridional Electric Fields From DE 2 During Solar Maximum

N. C. MAYNARD

Air Force Geophysics Laboratory, Hanscom Air Force Base, Massachusetts

T. L. AGGSON AND F. A. HERRERO

NASA Goddard Space Flight Center, Greenbelt, Maryland

M. C. LIEBRECHT

Science Applications Research Inc., Lanham, Maryland

Electric field data from the double probe vector electric field instrument (VEFI) on the DE 2 spacecraft have been analyzed to determine the average meridional electric field (zonal ion flow) patterns in the region between ± 30° magnetic latitude during solar maximum conditions. Over 300 passes were used to compile the data set. Data were projected to a constant 300-km altitude and to the equatorial plane assuming that the electric field along the magnetic field was zero. The average data set displayed a rapid increase of the downward meridional electric field with local time near 1800 MLT with the higher latitudes seeing the change first. A secondary nighttime maximum of this electric field component was observed post midnight with the crossover to upward electric fields (westward ion flow) occurring between 0400 and 0500 MLT. A sharp return to near zero was observed between 1200 and 1300. Typical average amplitudes range between 3 and 6 mV/m. No consistent variations with magnetic activity were observed. Although the daily variation in the zonal ion flow is dominated by the diurnal term, a net superrotation is evident in the harmonic analysis. The superrotation is strongest near the equator and decreases with latitude, because of the disturbance dynamo. The higher order harmonics up through the quatrediurnal term are also of significant magnitude in the analysis of the shape of the daily variation. Close similarity is seen to the zonal neutral winds indicating that they form the principal driving force. The magnitudes of the electric field derived ion drift are somewhat higher than the average F region neutral wind values. This along with the higher order harmonic content argues for the need to develop fully coupled E and F region model depicting the ionosphere and thermosphere interactions in a self-consistent fashion.

1. INTRODUCTION

Observations of meridional electric fields or zonal plasma flow at low and mid-latitudes have in the past been primarily made from incoherent scatter radar stations such as Jicamarca near Lima, Peru [*Woodman*, 1972; *Fejer et al.*, 1981, 1985], Arecibo in Puerto Rico [*Behnke and Harper*, 1973; *Ganguly et al.*, 1987] and Saint Santin [*Blanc and Amayenc*, 1979] to determine average ion drifts including seasonal effects. Observations of the drift of scintillation irregularity structures has also added limited ion drift data at night when spread F is present [*Abdu et al.*, 1985; *Basu et al.*, 1980]. The low latitude electric field measurements from the DE-2 satellite [*Aggson et al.*, 1987] provide a new more spatially extensive data source with coverage at all local times and longitudes.

The characteristics of equatorial zonal plasma flow have been summarized by *Fejer et al.* [1985] based on Jicamarca data. Westward drifts up to 50 m/s are typical of daytime hours while at night eastward drifts up to 130 m/s dominate. During the day F region dynamo effects [*Rishbeth*, 1971] are shorted to a large extent by the high conductivity in the E region, while after dusk the fields result from the coupled E and F region dynamos [see *Fejer et al.*, 1981]. The result is a rapid increase in the eastward drift just after local sunset. The equatorial eastward flow increases sharply with increasing altitude below the maximum of the F region, and the altitude of the steep gradient increases with increasing local time [*Kudeki et al.*, 1981; *Aggson et al.*, 1987]. *Fejer et al.* [1981] found that the zonal drifts have considerable day-to-day variability, but do not show significant changes with season or magnetic activity. This contrasts with the significant variations with magnetic activity seen in the east-west electric field or vertical drifts [see *Fejer*, 1981]. *Fejer et al.* [1985] did find increases in the nighttime maximum attributable to solar cycle variations. Most of the Jicamarca data presented are altitude averages from the 300 to 400 km altitudes and are treated as height-independent variations. Some latitude variations projected to the equator as altitude variations may affect their local time averages. *Fejer et al.* [1985] also found significant fluctuations on time scales of 5–10 min; however they cautioned about over interpreting these variations due to nonoptimized analysis procedures.

The ion drifts ($\mathbf{Vi}$) can be related to polarization electric fields ($\mathbf{E}$) by

$$\mathbf{Vi} = (\mathbf{E} \times \mathbf{B})\, B^2$$

Structures in the vertical profile of electric fields can in turn result from latitudinal variations which are projected along equipotential magnetic field lines to the geomagnetic equator. Thus measurements of the meridional electric field obtained from the polar orbiting DE 2 satellite can be projected to a

Paper number 7A9234.

latitudinal profile at constant altitude or to an altitude profile at the equator. *Aggson et al.* [1987] showed that in the evening the electric field above the equatorial *F* region peak decreased with increasing altitude or latitude. This effect had been predicted by Anderson and Mendillo (1983) in their coupled *E* and *F* region model.

E region dynamo models have been developed over the years to explain the daily variations of ionospheric currents derived from ground magnetometer measurements. Despite the apparent success of dynamo theory to model the currents, there is poor agreement with midlatitude electric fields deduced from ion drift measurements [*Richmond et al.*, 1976]. They added ion drag influences on the wind to the dynamo formulations to provide some improvement. In the more recent models of *Anderson and Mendillo* [1983] and *Takeda and Maeda* [1983] the self-consistent coupling of the *F* region dynamo [*Rishbeth*, 1971; *Heelis et al.*, 1974] with the *E* region dynamo in which field aligned current flow is allowed have resulted in better agreement with these data.

Richmond et al. [1980] have taken the radar data from Arecibo, Jicamarca, St. Santin and Millstone Hill for quiet periods $Kp \leq 2+$ and have empirically extrapolated to all latitudes, longitudes and local times using a polynomial expansion. Some seasonal dependence is factored into the model. The amplitude of the zonal drifts decreases with increasing latitude. A maximum of near 80 m/s is seen near 2100 MLT at 10° magnetic latitude and a mimimum of near 40 m/s westward drift is seen near 1100 MLT. Zero crossings are at about 0500 and 1600 MLT. The variation is principally diurnal.

The principal driving force for the ions at low and mid latitudes is the neutral wind. Recent measurements of the *F* region zonal neutral winds from DE 2 have shown a basic diurnal variation with a small superrotation term [*Wharton et al.*, 1984]. *Herrero and Mayr* [1986] have done a spectral analysis on both the DE neutral wind data and the Jicamarca ion drift data and found close correspondence on all terms except the superrotation term. The ions show larger superrotation in the equatorial region, since the westward daytime drift is smaller than the eastward nighttime drift due to *E* region loading.

In this paper we will use the spatially more extensive DE 2 electric field data set to provide an average picture of the low-latitude meridional electric fields or zonal plasma drift. These data make it possible to obtain latitudinal variations of the ion drift. The results will then be compared to those obtained from radar measurements and also to the DE 2 neutral wind measurements.

2. Data Handling

The Vector Electric Field Instrument (VEFI) on DE 2 [*Maynard et al.*, 1981] measured the electric field vector in the orbit plane. For the 90° inclination orbit this translates into the meridional component in both magnetic and geographic coordinates at low latitudes. The DE 2 spacecraft was three-axis stabilized with the electric field measurement axes at ±45° to the horizontal. Cylindrical antennas, each 11m in length, were extended in each direction on each measurement axis. The sensor part of each antenna was the outer 2 m making the baseline for the double floating probe measurement to be 21.4 m.

Previous studies with the instrument have primarily concentrated on the high-latitude data where electric fields are much larger. The measurement errors have been ±4mV m due to uncertainties in constant offsets in the measured potential difference usually referred to as "contact potential" [see *Maynard et al.*, 1982]. At high latitude the adjustment of a constant offset for each axis for the whole pass has been made assuming that the electric field is near zero at mid-latitude and that the integrated potential across the high-latitude region from mid-latitude on one side of the globe to mid-latitude on the other side is near zero. It was puzzling that a different "constant" was often needed for the southern hemisphere data compared to the northern hemisphere data on the same orbit. This question has been resolved by decomposing the low-latitude data into components perpendicular and parallel to the in orbit plane magnetic field from passes crossing the geomagnetic equator. Since the magnetic field is nearly in the orbit plane, one would expect the parallel component of the electric field to be almost exactly zero.

Figure 1 shows an example of DE 2 electric field data in which the contact potential adjustment has been determined such that the field aligned component E_z (lower panel) is near zero over most of the regions. The constancy of a near zero E_z within a broad latitude range and the symmetry of the resulting perpendicular component E_x (middle panel) about the geomagnetic equator testifies to the correctness of the adjustment.

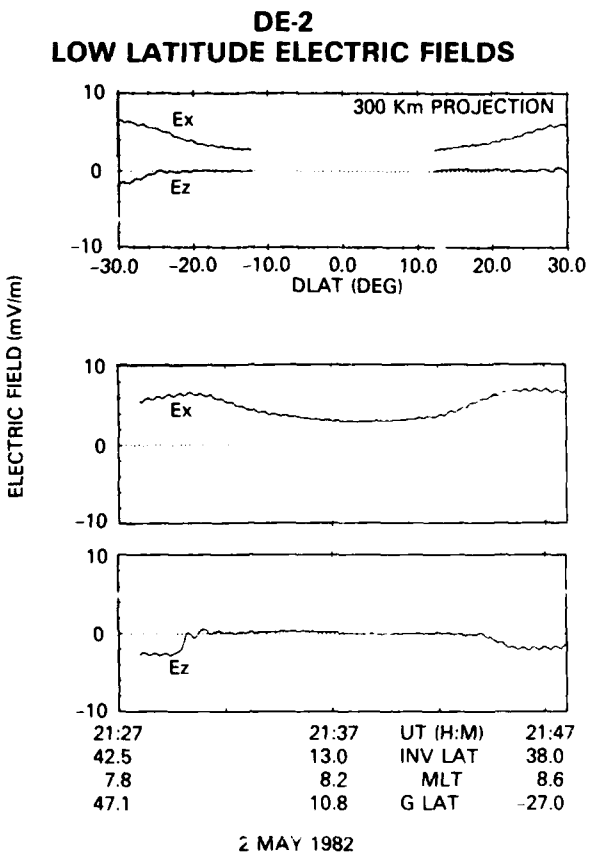

Fig. 1. The electric field measured by DE 2 in a magnetically oriented coordinate system. The bottom two panels show the meridional component (E_x) (positive poleward or outward) perpendicular to the in-plane magnetic field and the component parallel (E_z) to the in-plane magnetic field. The top panel shows the projection of these components along the magnetic field to a constant altitude of 300 km, assuming that the electric field along the magnetic field is zero, versus latitude.

At each end of the pass the E_z component deviates from zero. Examination of the data in the original measurement axes showed that each change occurred in data from one axis alone, and that it occurred only when that axis was nearly aligned with the magnetic field. Thus a contact potential change occurs whenever an axis passes through the magnetic wake of the satellite (i.e., away from the velocity vector and along **B**). Each axis will become nearly aligned with the magnetic field once in each low latitude passage explaining the differences in contact potentials for northern and southern high latitude regions. Causes of contact potential differences are primarily related to asymmetries in surface properties of opposite sensors either from contamination or geometry. Thus, the above implies asymmetric flow along **B** and deposition of contaminant ions from the spacecraft. Langmuir probes have experienced contaminant deposition over time, prompting the use of heaters to clean the probe surface of contaminants [see *Krehbiel et al.*, 1981].

By restricting the coverage of this study to ± 30 geomagnetic it was possible to automate the determination of the contact potential for each pass. The fact that the $\mathbf{V} \times \mathbf{B}$ electric fields which have to be subtracted are smallest near the equator reduces the effects of attitude errors. Furthermore, the fact that the contact potential is constant over this range allows us to reduce the measurement errors to ± 2 mV/m. Of the over 300 passes processed less than 2% could not be handled in an automated fashion with a constant contact potential. These were omitted from the study using the criteria that the $|E_z|$ must be less than 2mV m for the E_x data to be valid.

The meridional electric field values measured at varying altitude along the orbit track were projected along the magnetic field to a constant altitude of 300 km. This provides assuming $\mathbf{E} \cdot \mathbf{B} = 0$ a latitude local time map of E_x. Using the same argument, the electric field can be projected to 0° magnetic latitude giving the altitude profile of E_x at the geomagnetic equator. This is discussed in more detail below. The top panel in Figure 1 shows the 300-km projection. The gap at the center of the plot results from the altitude of the equator crossing being above 300 km. The precession of perigee around the orbit and the constancy of the orbit plane in inertial space causes certain local times to be only covered at equinox and others at solstice, and also restricts the data coverage inside $\pm 15°$ (latitude survey) or below 375 km (equatorial projection).

Figure 2 shows seven individual passes in the 0300–0400 MLT slot projected to 300 km constant altitude. No selection criteria were exercized except that of local time. The general consistency of the data from day to day and pass to pass is evident. A montage of passes from near 2000 MLT was presented by *Aggson et al.* [1987] (their Figure 2). Again, the overall consistency of the latitude profiles at a particular local time was demonstrated from pass to pass. Typical profiles versus latitude are shown in Figure 3 for every 2 hours over the 24-hour day. Systematic changes with local time are evident.

For most passes the electric field is regular and well behaved. In a few cases during magnetic storm periods spread F irregularities increased to the point of dominating the dc electric field. Figure 4 shows an example near 2000 MLT. Note the change in scale. Even though, the irregularities reach nearly 20 mV m, the background electric field is still in the 5–10 mV m region which is typical for that local time. The

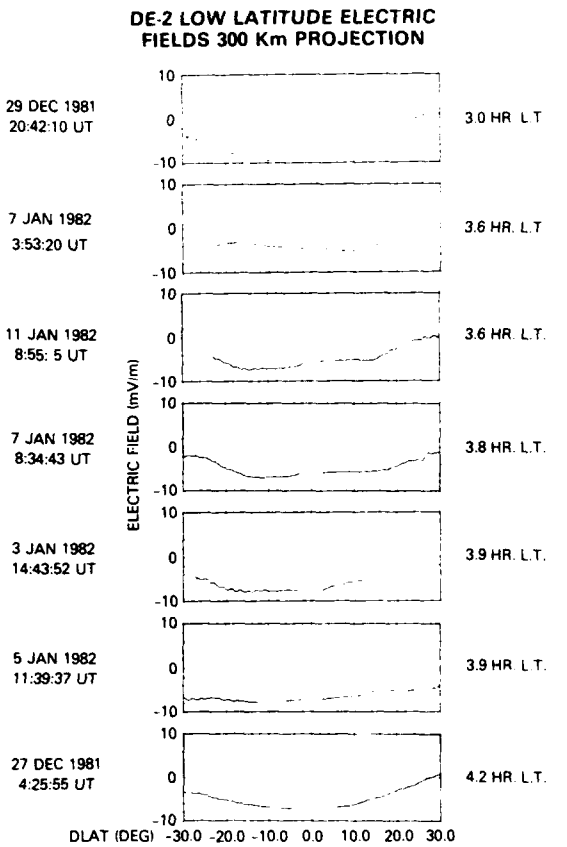

Fig. 2. A collection of projected perpendicular electric field (positive poleward or outward) profiles spanning about one hour of local time illustrating the repeatability of the data at a particular local time.

regions of spread F are not conjugate in the plot and should not be expected to be as they are local and not necessarily extended in longitude. Both time and spatial variations work against the probability of actually observing conjugacy on a given pass. The remainder of the paper will concentrate on the average electric field as this type of activity is not typical and does not grossly distort the averages.

3. Average Patterns

In order to establish a statistical picture of the meridional electric field at low latitude, all projected data were averaged in 5° latitudinal bins (300-km projection) and 25-km altitude bins (equatorial projection). The results were then combined and averaged for each hour of local time. Three hundred and two passes were used in this study covering all local times. Because of the afore mentioned nonuniform orbital coverage and a preponderance of passes in the 19hr time frame used in the previous study [*Aggson et al.*, 1987] the statistics are not uniform. Table 1 shows the distribution of data points with latitude north and south of the equator. At any given latitude, each point represents a separate pass. Conjugate symmetry has been assumed and the northern and southern hemisphere data sets have been combined for the equatorial projection.

The resulting data sets were averaged for each magnetic local time latitude bin and are displayed in Figure 5 for the latitudinal projection and Figure 6 for the vertical or equatorial projection. The vectors are rotated into the horizontal east-west drift direction for each of displaying and to show the

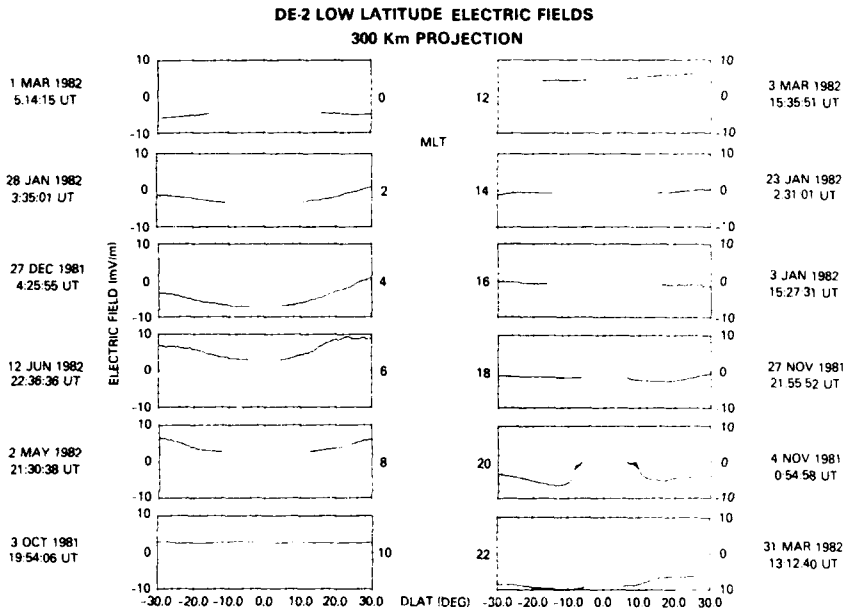

Fig. 3. Examples of latitudinal profiles of the projected perpendicular electric field (positive poleward or outward) for every 2 hours to illustrate the diurnal variation. The variability of the gap at the magnetic equator is a result of the local time coverage being a function of season and of the change in the latitude of perigee with time.

related motion. Actual meridional electric field values and the standard deviation of each average are given in the appendix.

Several characteristics stand out in the patterns:

1. The electric field increases rapidly with local time near 1800 hrs with the higher latitudes (or altitudes in the equatorial projections) seeing the increase first. This was discussed by *Aggson et al.* [1987].

2. The downward electric field (eastward drift) decreases near midnight and then increases again before the reversal to westward drift between 0400 and 0500 MLT.

3. Electric fields are upward corresponding to westward drifts in the morning hours.

4. A sharp return to near zero electric fields is observed between 1200 and 1300 MLT. The electric fields remain near zero during the remainder of the afternoon.

5. Average electric field magnitudes range up to 8 mV/m with 3–6 mV/m being typical for most local times.

6. The integrated areas under the eastward drift portions of the curves are larger than those under the westward drift portions indicating that a net superrotation term is present. This unbalance is greatest at the lower latitudes.

7. The zonal ion drift is approximately symmetric with respect to the geomagnetic equator (some seasonal asymmetries are possible but not separable). These features will be discussed and compared to other results in subsequent sections.

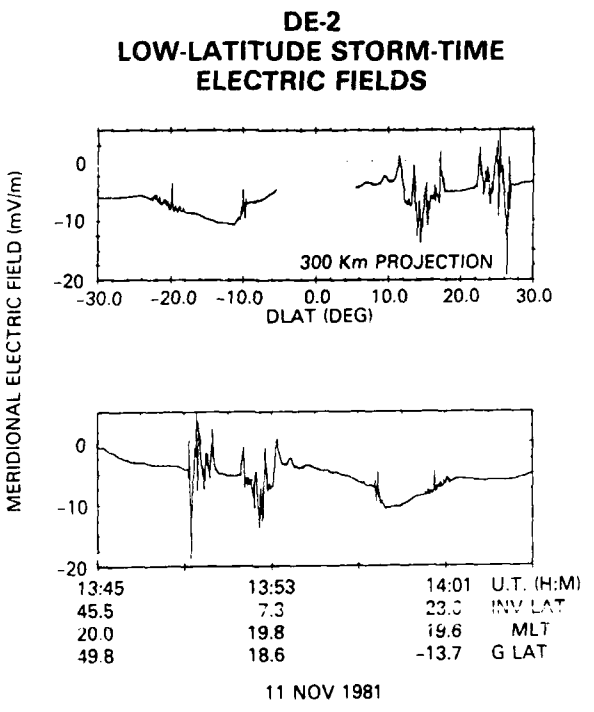

Fig. 4. A pass from a magnetically active period containing very large variations in the electric field related to spread *F*. The bottom panel shows the orbital variation as taken with time while the top panel shows the same data projected to a constant 300-km altitude versus magnetic latitude. Note that even though the variations are large, the background electric field is comparable to that seen on other passes at the same local time.

Several words of caution relative to the data set need to be emphasized. The local time coverage is determined by the rotation of the orbit with season. Thus data from 1800–2200 and 0600–1000 MLT is primarily solstice data, while equinox data is emphasized in between. The solstice data is further biased toward December data because of the abundance of perigee data near the equator during December 1981. The movement of perigee around the orbit plane results in the lack of low altitude data at some local times and an incomplete data set with local time at <5 magnetic latitude. Thus seasonal variations can not be separated out. The high degree of symmetry displayed with respect to the equator is indicative of equipotential magnetic field lines and or little seasonal variation resulting from solstice. We assume that the 24-hour variations obtained here can be used to estimate latitudinal vari-

TABLE 1. Data Distribution for Low-Latitude Meridional Electric Fields

Latitude	MLT, Hours																							
	0100	0200	0300	0400	0500	0600	0700	0800	0900	1000	1100	1200	1300	1400	1500	1600	1700	1800	1900	2000	2100	2200	2300	2400
−30	9	10	5	6	4	8	10	6	9	12	9	10	14	5	9	13	10	21	23	17	5	6	5	4
−25	8	11	3	11	3	9	11	9	7	14	7	13	13	8	7	14	11	21	28	17	6	8	9	11
−20	10	10	6	14	7	13	13	9	6	14	11	11	15	8	10	13	13	19	32	21	6	7	17	11
−15	10	10	6	15	6	13	6	9	7	16	10	14	14	8	8	9	13	18	35	23	5	5	16	8
−10	3	7	6	13	5	11	4	4	9	13	8	10	9	4	7	10	4	11	34	23	4	5	1	9
−5	0	4	4	12	1	10	3	1	8	9	3	10	5	1	3	1	3	1	37	8	4	2	1	8
0	0	0	0	0	0	0	0	0	0	0	0	0	0	0	0	0	0	0	0	0	0	0	0	0
5	0	3	5	11	4	8	3	1	8	8	3	10	5	1	3	1	3	2	35	9	4	1	1	8
10	2	7	5	15	8	8	5	3	9	11	11	9	8	3	8	9	5	10	36	23	4	4	1	8
15	8	10	9	13	9	10	7	8	9	11	18	12	10	9	8	11	11	15	40	20	5	4	15	9
20	9	8	11	13	8	10	12	11	7	10	14	13	8	9	12	16	11	16	38	19	3	8	16	11
25	9	8	9	11	8	7	9	10	6	10	12	11	6	9	12	15	12	15	27	17	2	8	14	12
30	7	6	9	7	4	7	7	9	7	9	10	7	8	8	11	9	7	10	25	15	3	8	12	9

ations of tidal components which correspond to a mixture of equinox and northern hemisphere winter for the years 1981–1982.

In early analyses of the data set it was noticed that there was a distinct variation with longitude. Larger electric field values were found in regions where the Earth's magnetic field was higher. All values were therefore individually converted to drift and reaveraged to obtain the pattern shown in Figure 7.

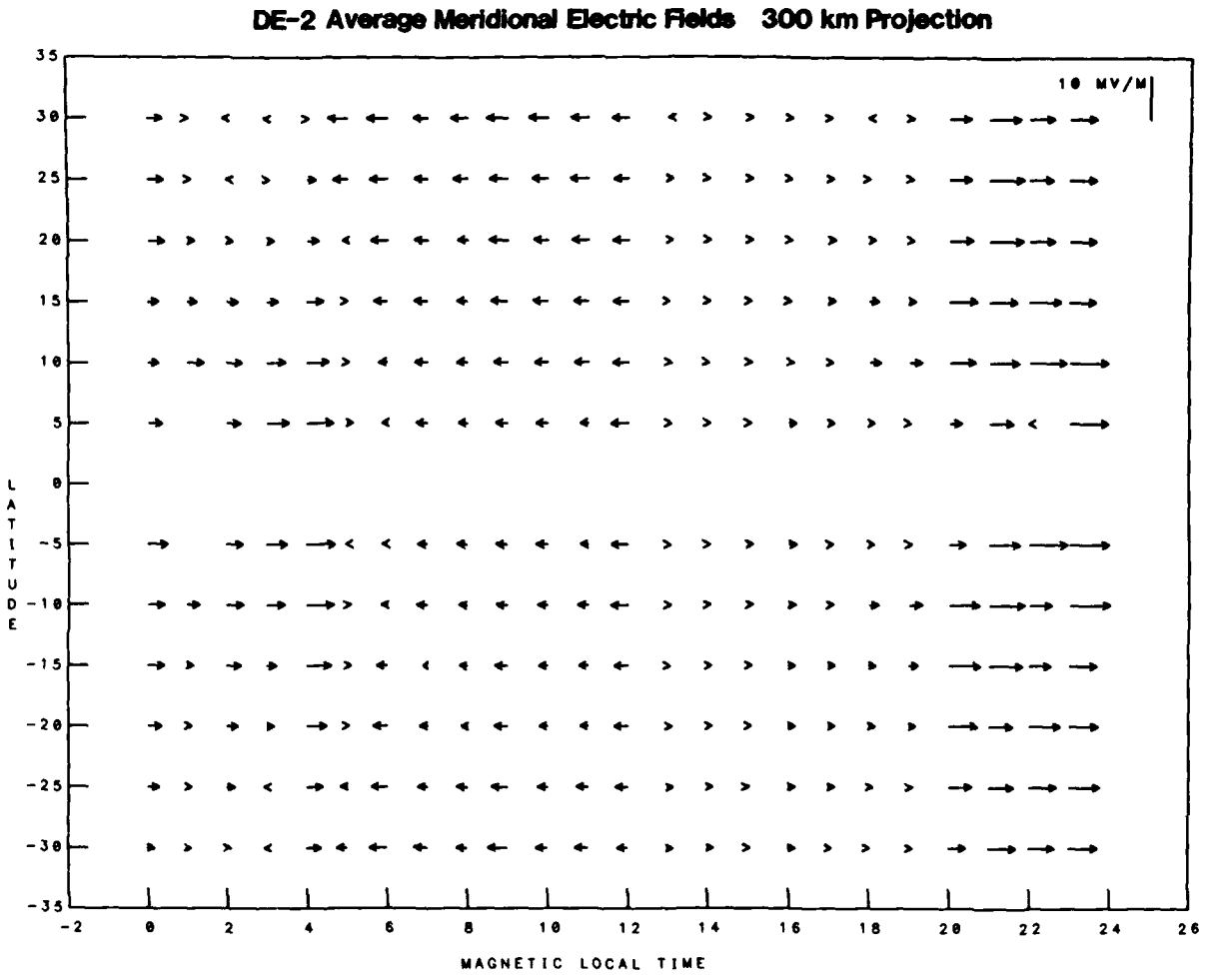

Fig. 5. The average meridional electric field at 300 km based on DE 2 electric field measurements. The vectors have been rotated into the direction of the corresponding zonal ion drift for clarity of presentation. All vectors are therefore horizontal since the zonal component of the electric field was not measured, hence could not be included. The scale in electric field units is at the top right. Data from all longitudes are average together (see text).

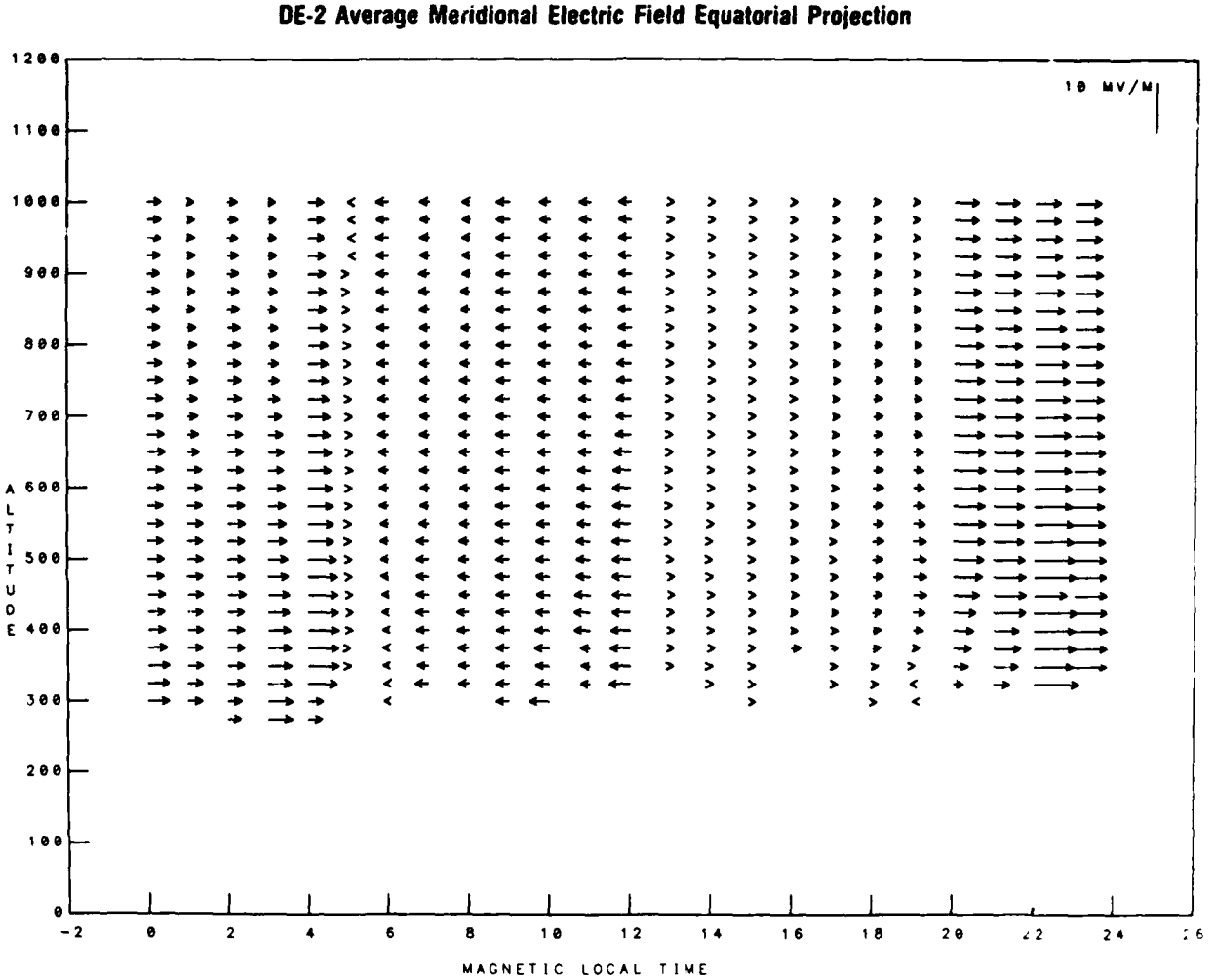

Fig. 6. The average meridional electric field projected along the magnetic field to the equator and shown versus altitude. The vectors have been rotated into the ion drift direction for clarity (see Figure 5 caption).

This pattern is invariant with longitude within the accuracy of the data, affirming that the neutral wind driven ions move consistently at all longitudes and that the electric field longitudinal variations are created by longitudinal changes in B in the expression $\mathbf{E} = -\mathbf{V} \times \mathbf{B}$. Average drift values are also given in the appendix.

4. Comparisons to Other Data

To facilitate comparison with other data sets, the average zonal-drift values for the northern hemisphere have been plotted versus local time in Figure 8. The increase starting at 1800 MLT and the secondary peak near 0400 MLT are clearly seen. Note that the secondary peak near 4 hrs decreases as one gets farther from the equator. The return to zero magnitude near 1200 hrs is prevalent at all latitudes.

Figure 9 shows the average eastward drifts measured by the Jicamarca backscatter radar facility [*Fejer et al.*, 1985]. The curve is for solar max conditions which best corresponds to the solar cycle phase of the DE data. The averaged zonal drift data for 10 N magnetic latitude from DE is also plotted for comparison. Note that the Jicamarca data is collected from 300 to 650 km in altitude, with 350 km being the most typical altitude for the average values that are plotted. The secondary peak near 0400 MLT is evident in both data sets although it is more prominent in the DE data. The Jicamarca magnitudes are 25 to 50% less than the DE values. The most pronounced difference between the two curves is the gradual return to eastward drifts in the early afternoon with the zero crossing near 1600 MLT observed at Jicamarca compared to the more abrupt transition to near zero in the DE data. While the range of values shown by *Fejer et al.* [1985] for early afternoon easily encompasses zero, their average clearly remains westward.

Ganguly et al. [1987] have published average zonal drift values derived from backscatter data taken at Arecibo, which is at 32 N geomagnetic latitude. Amplitudes range from near −20 to near +30 m/s, well below the DE values. The Arecibo data is primarily from solar minimum conditions. *Fejer et al.* [1985] have shown a considerable solar cycle effect in the Jicamarca data with solar maximum values being 50–75% larger than those from solar minimum. The secondary nighttime peak near 0400 MLT is not seen at Arecibo consistent with the DE data at +30° magnetic latitude, with the transition to westward drifts at Arecibo occurring between 1000 and 0400 MLT depending on season. The Arecibo data set does show the return to near zero in the drift at noon in the equinox data. The DE data in the noontime and early afternoon periods are equinox data; thus the two data sets confirm the

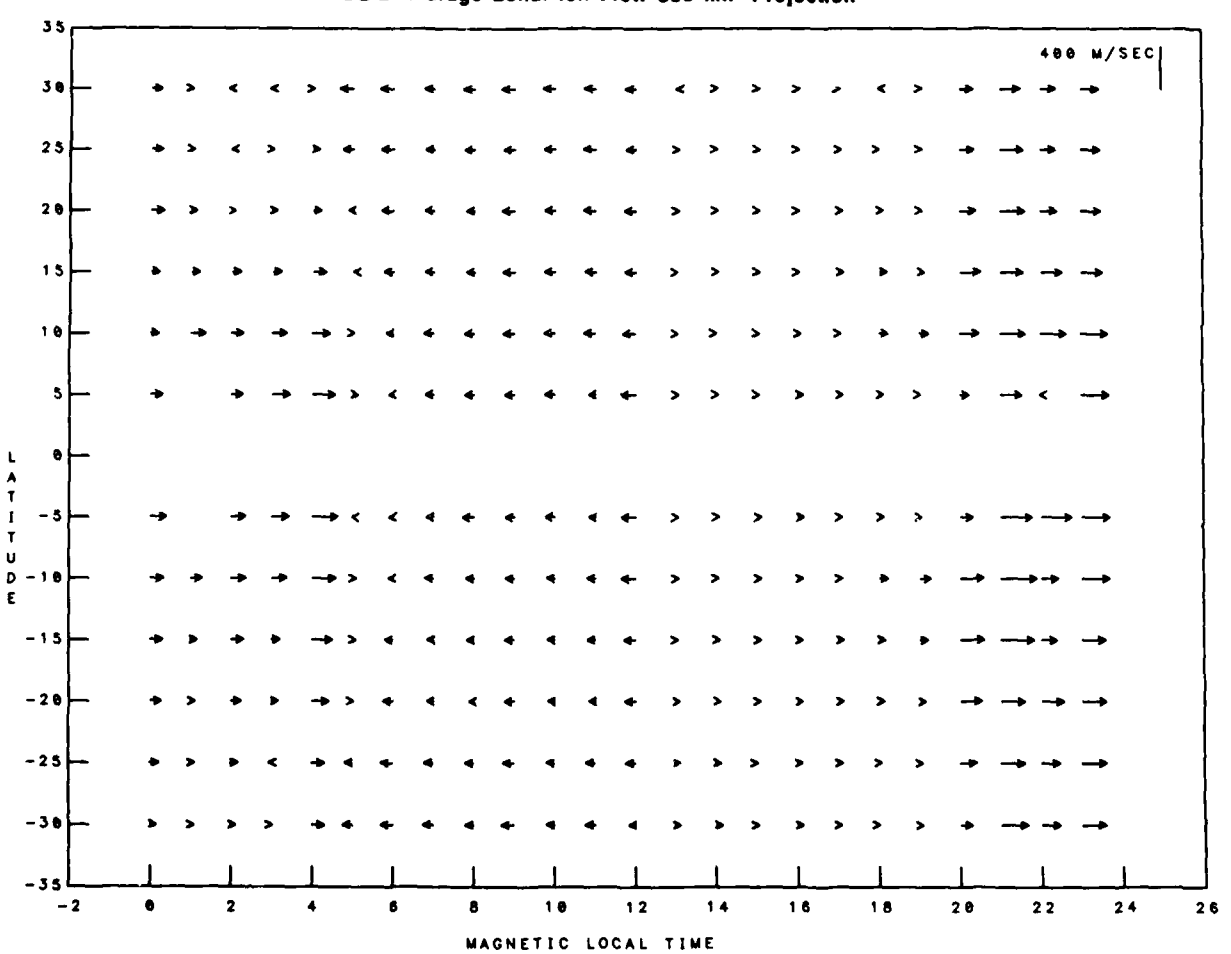

Fig. 7. The average zonal ion flow from individual pass conversions of the meridional electric field to zonal flow. Data from all longitudes are included.

noontime decrease at mid-latitudes. *Fejer et al.* [1981] did not find similar behavior with season in the equatorial Jimarca data set. The Arecibo summer data also shows a crossover to eastward drifts near noon and also a very different early morning behavior. Their summer local maximum in the westward drift near 0300 LT would not be reflected in the DE data, as equinox controls that portion of local time.

Figure 10 compares the average zonal neutral wind variations from the DE 2 neutral wind and temperature spectrometer (WATS) instrument at the geographic equator for 350-km altitude with the VEFI data. The VEFI error bars correspond to the statistical fluctuation of the data. These should be added in a RMS fashion to the previously mentioned ± 2 mV/m or $\sim \pm 70$ m/s measurement uncertainty after it has been reduced by the square root of the number of samples (see Table 1). The diurnal pattern of this plot corresponds the closest to ion drift values derived from the VEFI electric field data (Figure 8). The shape is very similar to that of the zonal ion flow with the exception of the post noon period. The ion flow magnitude is typically equal to or larger than the neutral wind magnitude. Note that the wind data corresponds the geographic equator while zonal ion drift values are keyed to the geomagnetic equator. The close similarity of the two data sets especially at night again points to the neutral wind as a principal driving force; however, the somewhat larger ion velocity at some local times presents a problem with this interpretation (a topic that will be addressed further in the discussion).

5. Fourier Analysis

The DE data are representative of equinox and northern hemisphere winter, and the average 24-hour variations obtained show a high degree of symmetry with respect to the geomagnetic equator. Hence assuming that the average 24-hour variations represent a mixture of these two seasons, an estimate of the latitudinal variation of some of the tidal components of zonal ion-drift can be determined through Fourier analysis. The average daily variations of the ion drift have been Fourier analyzed at each latitude interval from 10° to 30° in each hemisphere. Figure 11 shows the average daily variations obtained at 15° and 30° magnetic north latitudes from fourth-order Fourier series expansion of the corresponding data shown in Figure 7. The tidal amplitude spectra for both latitudes are shown in the lower panel. Table 2 gives the amplitudes and phases up through the fourth order for each latitude as well as the neutral wind values based on DE 2 WATS data [*Herrero and Mayr*, 1986]. Superrotation is represented by the prevailing term $A(0)$ in the spectra. Accordingly, the amplitude spectra show that $A(0)$ at 15° is significantly larger than $A(0)$ at 30° showing that the ions superro-

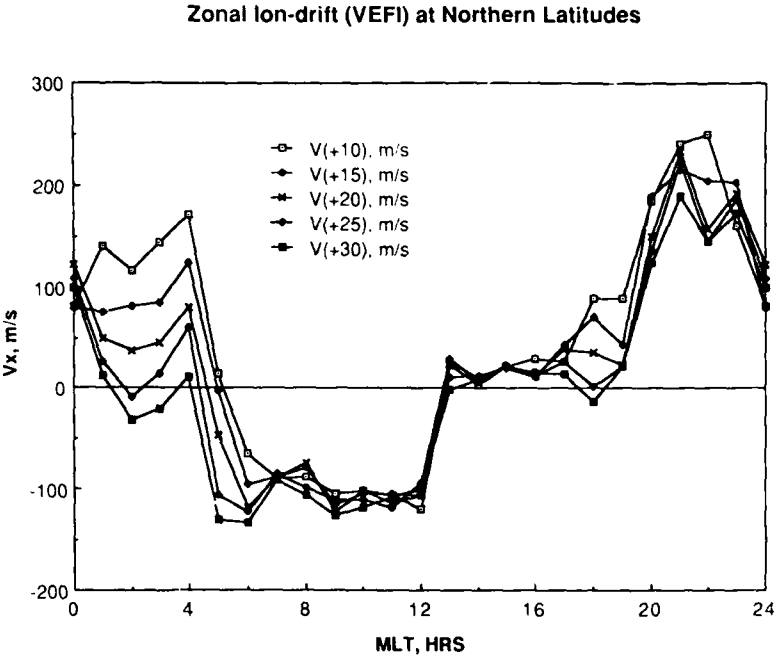

Fig. 8. Line plots of the zonal ion flow versus magnetic local time. The numbers in parentheses after V give the latitude represented by each curve.

tate more rapidly at 15° than at 30°. We note also that the harmonic terms up to and including the fourth order have moderately large amplitudes, the semidiurnal $A(2)$ being smaller at 15° than at 30°. The latitudinal variations of these five significant terms are shown in Figures 12, 13 and 14. Figure 12 shows the latitudinal variation of the prevailing or superrotation term $A(0)$, and Figure 13 shows the latitudinal variation of the diurnal amplitude $A(1)$ and its phase. The semidiurnal, ter-diurnal and quatre-diurnal amplitudes are shown in Figure 14. Except for the semidiurnal term $A(2)$, all amplitudes are strongest near the geomagnetic equator. However, all components, including $A(2)$, are reasonably symmetric about the equator. Deviations from symmetry probably arise from seasonal variations in V_x at certain local times and from the mixture of seasons over the 24-hour period as described in section 2 above.

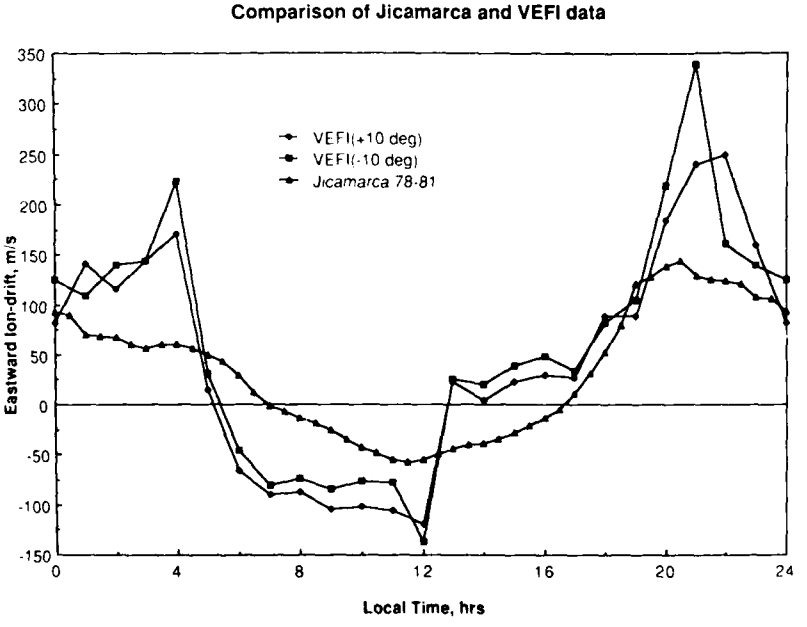

Fig. 9. Comparison of ion drifts determined from the Jicamarca radar facility and from the DE 2 electric field data. The Jicamarca data [after *Fejer et al.*, 1985] is from the active period of the solar cycle although spanning a broader period and not completely overlapping. The 10° latitude curves from DE project near the typical altitude represented by the Jicamarca measurements.

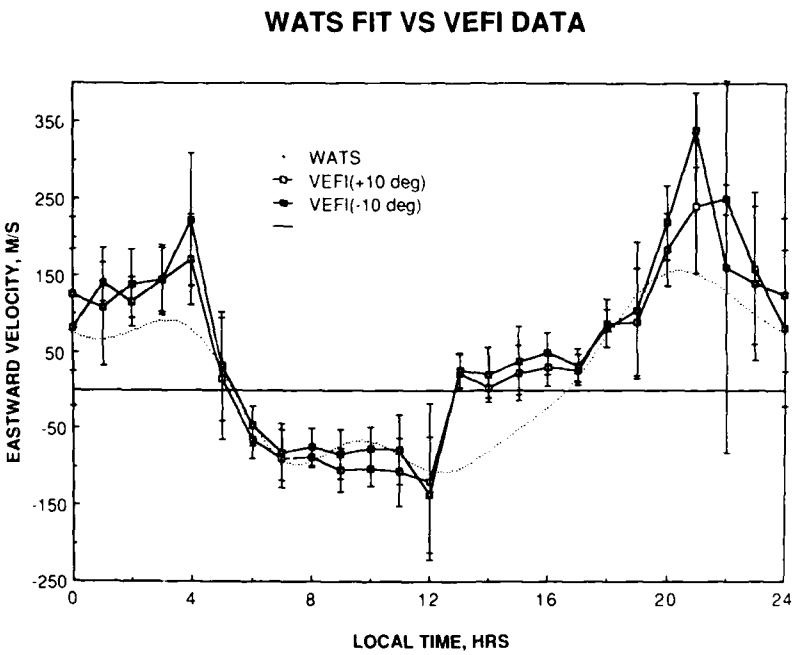

Fig. 10. Comparison of average zonal wind measurements from the WATS instrument on DE 2 [after *Wharton et al.*, 1984] with the average ion drifts determined from the VEFI electric field data. The two data sets were independently assembled with an unknown degree of overlap. The error bars on the electric field data represent the statistical fluctuation of the data.

6. Discussion

A definite ion superrotation is an obvious feature of the data. An examination of Figure 8 clearly shows more integrated area under the curves above zero than below for all except the highest latitude curves. The harmonic analysis zeroth order term displayed in Figure 12 indicated an average value of 48 m s for the region inside ±15°. *Wharton et al.* [1983] found a neutral superrotation of 10 m s from the DE-2 WATS data, while *Woodman* [1972] detected an ion superrotation of about 30 m s in the Jicamarca data. *Herrero and Mayr* [1986] showed that the ion superrotation amplitude from Jicamarca data increased with solar activity, with 33 m s being applicable to the 1978–1981 period. The DE data corresponds to higher solar activity, being more nearly centered on solar maximum.

The latitudinal variation of the ion superrotation is perhaps the most significant feature of these data. Examination of the individual plots for each magnetic latitude in Figure 8 (and also in Figure 12) shows that the ion drifts are strongly eastward at low latitudes in the postmidnight to morning sector, and at latitudes near 30° the corresponding drift is small and possibly westward. It is known that the ionosphere subrotates during strong geomagnetic disturbances, as noted and explained by *Blanc and Richmond* [1980] in terms of the disturbance dynamo. In the absence of magnetic disturbances there still exists a quiescent level of auroral heating. Indeed, such a heat source has been regularly hypothesized in order to understand thermospheric circulation phenomena [*Dickinson et al.*, 1975, 1977]. A constant auroral heat source would produce winds initially moving equatorward, but turning westward due to the strong Coriolis force component at high latitudes. Presumably this westward flow develops in such a way that it decreases with latitudinal displacement from the auroral region. Thus when interacting with the diurnal and prevailing zonal drifts excited at the equator, the westward flow originating in the polar region would impose a tendency to buck the net eastward flow in the ions, thus producing the gradual decrease in superrotation with increasing latitude.

A striking feature of the daily variation in Figure 8 is the abrupt abatement of the westward flow that occurs near local noon. A similar abatement, though not so abrupt occurs at equinox and in summer in the Arecibo data [*Ganguly et al.*, 1987] and also in the St. Santin observations [*Blanc and Ameyenc*, 1979], thus establishing this feature as characteristic of mid-latitudes at equinox. This is different from the equatorial Jicamarca data which has a more gradual transition (see Figure 9). Figure 8 shows that this feature is present at all latitudes in the VEFI data from 10° to 30°. As discussed in section 3, the VEFI data around local noon where the abatement is seen are equinox data corresponding to the Arecibo results. Since no longitude variations are detectable and since the sample distribution is relatively uniform, the VEFI data suggests that the Ganguly et al equinox feature extends toward the equator. This extension into the region where the DE 2 WATS *F* region netural wind data does not see the abatement suggests that it may be *E* region controlled.

The harmonic analyses (see Figure 11 and Table 2) indicate that the diurnal, ter-diurnal and quatre-diurnal terms all maintain relatively constant magnitude (peaking slightly near the equator) and phase with latitude, while the semidiurnal term decreases as the equator is approached. *Herrero and Mayr* [1986] also found a smaller semidiurnal term compared to the ter-diurnal term in their harmonic analysis of the DE 2 WATS neutral wind data for the geographic equator. The shifting of the phase of the larger semidiurnal term to earlier local times at higher latitudes, its reduced magnitude at lower latitudes, and an increase in phase with latitude for the higher

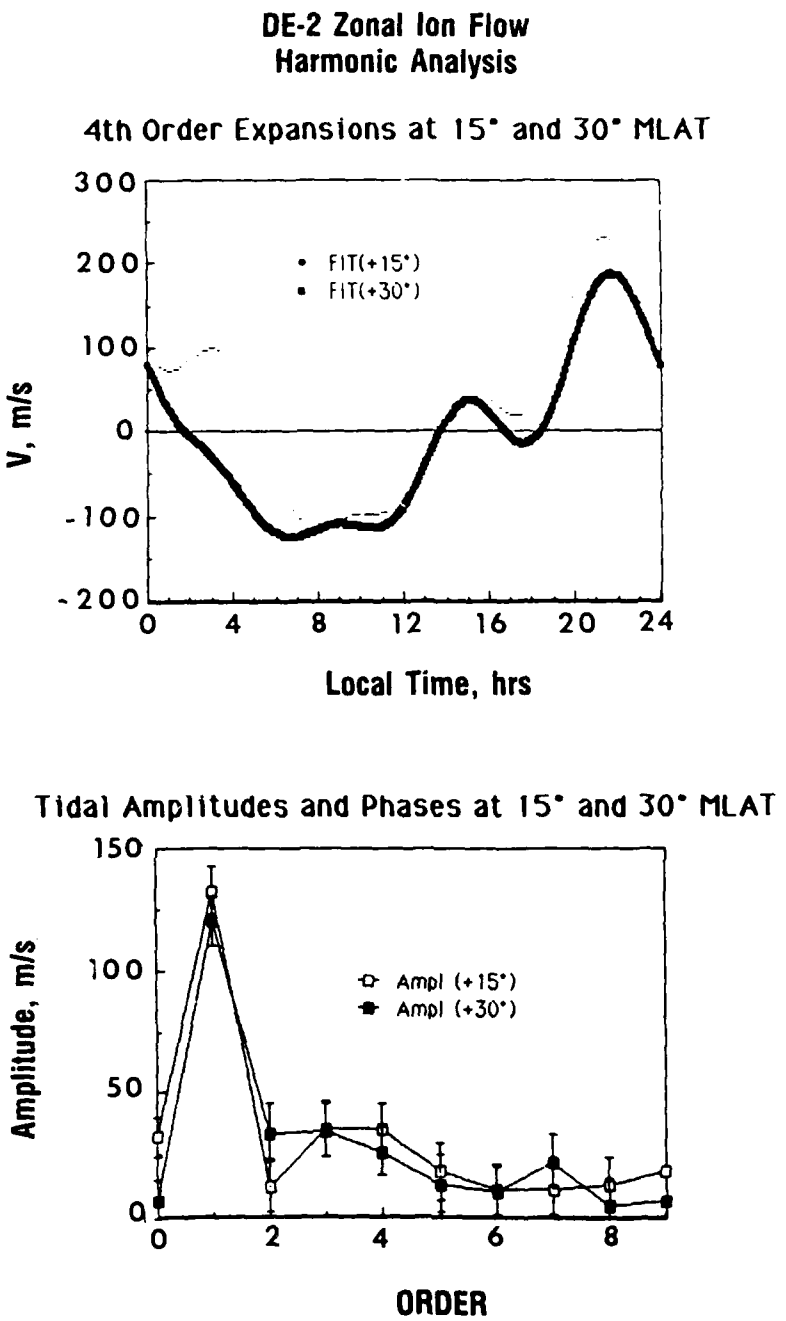

Fig. 11. The harmonic analysis of the zonal ion flow. The bottom panel represents the amplitude versus harmonic number with 1 referring to the 24-hour diurnal variation. The top panel displays the resulting curves for 15° and 30° north latitude data when the terms through fourth order are included.

order harmonics apparently results in the decrease in the secondary nighttime peak near 0400 MLT with increasing latitude (compare the fits for 15° and 30° in the upper panel in Figure 11, Table 2, and the corresponding data curves in Figure 8). The origin of the higher-order harmonics can be in the form of the basic solar forcing function or from modal coupling due to nonlinearities in the system and to interhemisphere coupling. *Herrero et al.* [1983] found significant amplitudes in the higher order harmonics in their tidal analysis of the thermospheric midnight temperature maximum which is related to the driving term for these drifts through the neutral density variations. Again in that data set the ter-diurnal amplitudes were sometimes larger than the semidiurnal amplitudes. Caution in over-interpreting the higher order harmonics should be taken in light of their low magnitude and the seasonal variability in the Arecibo data [*Ganguly et al.*, 1987] which is obviously mixed into in this analysis.

Forbes and Gillette [1982] provided a compendium of theoretical atmospheric tidal structures based on diurnal and semidiurnal terms. The upper thermosphere diurnal components

TABLE 2. Harmonic Analyses Amplitudes and Phases

Magnetic Latitude, deg	A(0), m/s	A(1) (PH1), m/s (hour)	A(2) (PH2), m/s (hour)	A(3) (PH3), m/s (hour)	A(4) (PH4), m/s (hour)
		Zonal Ion Drift Velocity			
−30	19	112 (20.8)	32 (0.3)	38 (16.3)	33 (13.2)
−25	32	116 (21.2)	37 (−0.3)	37 (16.8)	30 (14.0)
−20	47	120 (21.7)	25 (−0.1)	37 (15.4)	38 (13.4)
−15	54	128 (21.9)	12 (1.3)	41 (14.5)	40 (12.6)
−10	59	134 (22.3)	22 (7.4)	46 (13.4)	50 (11.8)
10	46	141 (22.3)	16 (5.4)	41 (14.4)	41 (12.8)
15	32	133 (21.9)	12 (1.6)	36 (15.3)	36 (13.4)
20	17	122 (21.5)	23 (0)	29 (17.4)	28 (12.8)
25	4	117 (21.2)	28 (−1.0)	33 (18.1)	26 (12.4)
30	7	120 (20.8)	34 (−1.7)	35 (18.4)	26 (12.6)
		Wind Velocity [From Herrero and Mayr, 1986]			
Geographic Equator	10	119 (22.7)	18 (15.4)	32 (11.0)	20 (14.0)

are of lower magnitude (nearer 70 m/s) but within about an hour in phase depending on the altitude (the theoretical phase is equal to our average value at 180 km and about one hour less at 300 km). Their solar semidiurnal tide is of the order of 30 m/s with nearly the same phase variation that is observed here with latitude for 300-km altitude. However, the amplitude variation with latitude of the *F* region semidiurnal term was either constant or peaking near the equator. The *E* region semidiurnal term is larger at mid-latitudes with an 8–10 hour phase difference. In general, the Forbes and Gillette tidal structure is diurnally dominated in the upper thermosphere with that domination increasing with latitude. Note that the semidiurnal term is the principal term in the *E* region (see also *Richmond et al.* [1976]). The diurnal domination of the VEFI derived ion drifts with similar phase to the theoretical structure indicates that the *F* region dynamo plays a major role in the electric field structure. The variation of the semidiurnal term and the coupling of the higher harmonics is indicative that the coupling to the *E* region may also be important factor, especially near noon were a strong mid-latitude *E* region semidiurnal term could play a large role in decoupling the ion drifts from the *F* region neutral winds.

The largest difference between the electric field derived drift velocities presented here and previous results, both theoretical and experimental, is in the amplitude. The generally higher values reported here compared to the radar measurements can to some degree be explained by differences in solar cycle, the day-to-day variability in the data, and limitations in the sizes and overlap of the data sets. The hardest difference to explain is the comparison with the WATS data in Figure 10. Both data sets are from the same satellite, although they were handled differently (geomagnetic focus versus geographic focus) and the pass selection was different. As can be seen from figure 10, the largest discrepancy, irrespective at the error bars, between VEFI and WATS data set is that the night time averaged plasma drifts from this study up to 100 m/s larger than the neutral wind velocities as averaged in the WATS study

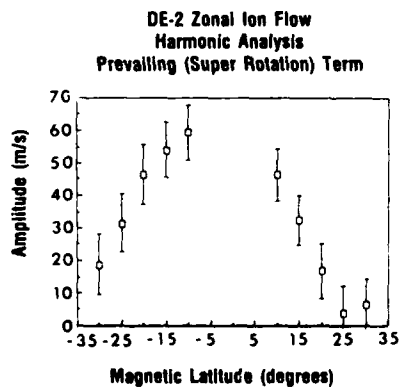

Fig. 12. The variation of the prevailing or super rotating zonal ion flow with magnetic latitude.

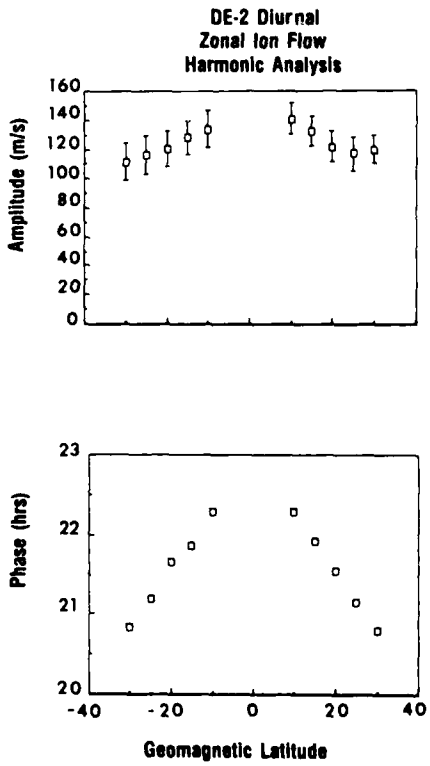

Fig. 13. The diurnal zonal ion flow and its phase versus magnetic latitude.

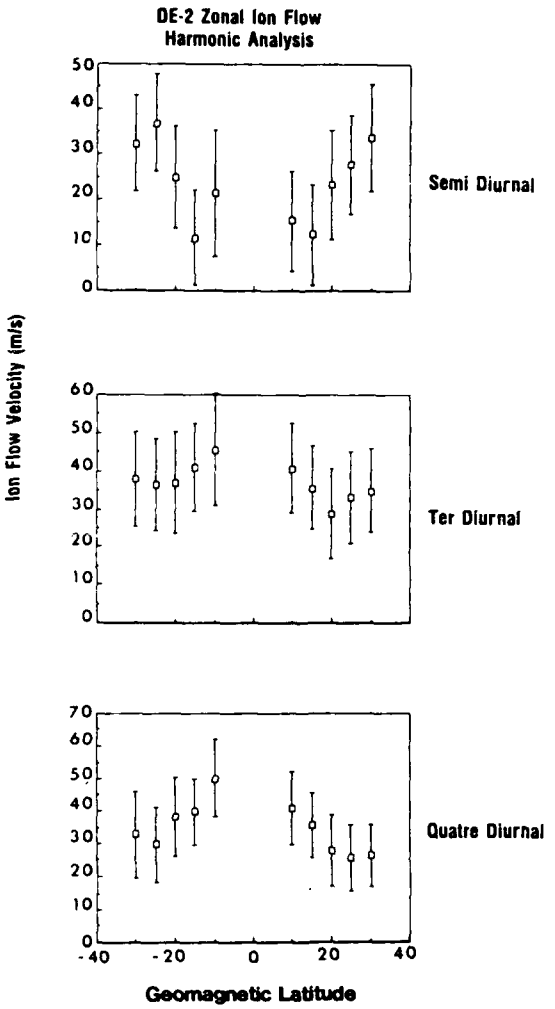

Fig. 14. Variations of the semidiurnal, ter-diurnal and quatre-diurnal harmonics in the zonal ion flow with magnetic latitude.

[*Wharton et al.*, 1982]. The largest differences occur 2 hours after sunset and 2 hours before sunrise. However, the periods of largest discrepancy are also periods at the largest error bars, (±100 m/s). More exact comparison between the averages of this study and that of Wharton et al. should properly include in the future, orbit by orbit comparisons rather than simple averages. In the Fourier domain, as can be seen from Table 2, the primary difference show up in a larger superrotation term and a slightly larger diurnal term. We would have anticipated that the nighttime ion drifts would have been comparable to the winds (not larger), while the daytime drifts would have been smaller than the winds (not comparable), based on the daytime shorting of the *F* region dynamo [*Rishbeth*, 1971] by the daytime *E* region conductivity. This mechanism creates a larger superrotation term but requires a smaller diurnal term. While it was noted by *Fejer et al.* [1985] that ground-based neutral wind measurements were typically less than the Jicamarca ion drift measurements, they also pointed out as the cause that the ground based wind measurements were related to a lower altitude (near 180 km). A similar magnitude problem exists in comparison to the theoretical calculation of *Forbes and Gillette* [1982] in that their magnitude for the diurnal term is less. The inaccuracies in the measurement (+2 mV m or about +70 m s) when added in RMS fashion to the statistical variations shown in Figure 10 allow most of the WATS curve to lie within the error bar envelope or at larger magnitudes; however, the basic trend for higher drift values is evident. The validity of this trend can only be examined through self consistently coupled calculations of the ionosphere and the thermosphere involving both the *E* region and the *F* region, since sources and sinks in both regions are involved.

7. Summary

Electric field data from over 300 equatorial passes of the DE 2 satellite have been analyzed to produce average meridional electric field or zonal ion flow patterns for the region between ±30 geomagnetic latitude. Several characteristics stand out:

1. The downward meridional electric field increases rapily with local time near 1800 MLT with the higher latitudes (or altitudes in the equatorial projection) seeing the change first (see also *Aggson et al.* [1987]).
2. The downward electric field (eastward drift) decreases near midnight and then has a secondary maximum before reversing to upward electric field (westward drift) between 0400 and 0500 MLT.
3. A sharp return to zero electric field is observed between 1200 and 1300 MLT and the electric field remains near zero throughout the remainder of the afternoon.
4. Average electric field magnitudes range up to 8 mV m with 3–6 mV/m being most typical.
5. In general, the small-scale spatial variations seen in individual passes are smaller in magnitude than the large-scale electric fields except during periods of large magnetic activity.

From harmonic analysis of the daily variation at each latitude, the following is inferred:

1. A net superrotation exists which is strongest at the lowest latitudes.
2. The basic variation of the ion flow is dominated by the diurnal term which is nearly constant with latitude.
3. The semi-diurnal term is weakest at the equator indicating a mixing of *E* and *F* region sources.
4. The third- and fourth-order tidal terms are also significant and apparently, along with the larger mid-latitude *E* region semidiurnal term, are related to the rapid return to zero post noon. This feature in the data is also seen in the Arecibo and St. Santin drift data.

No significant variation in the meridional electric fields with magnetic activity was observed consistent with previous results. Seasonal dependencies are inferred but not separable with this data set. An apparent longitudinal dependence in the electric field was shown to have been the result of the interaction of a longitudinal-dependence-free ion velocity and the Earth's magnetic field.

The amplitudes of the electric field are somewhat higher than would be expected when compared to the neutral wind measurements from DE 2 based on present understanding of the *E* and *F* region dynamos. The general pattern consistency with both neutral wind measurements and with theoretical analyses tends to confirm the winds as the source of the electric fields. There is, however, no self consistent calculation that couples the *E* and *F* region sources. Such a calculation will be necessary to understand the apparent amplitude discrepancy and to establish the means by which the higher harmonics are created and the role that they play.

Appendix

The values for the average patterns presented in Figures 5–7 are given in Tables A1–A4. Table A1 shows the meridional

TABLE A1. Average Meridional Electric Fields and Standard Deviations (300-km Projection)

	MLT, hours																							
Latitude	0100	0200	0300	0400	0500	0600	0700	0800	0900	1000	1100	1200	1300	1400	1500	1600	1700	1800	1900	2000	2100	2200	2300	2400
−30 EX	−1.0	−1.1	0.4	−3.5	2.4	4.3	3.0	2.5	4.4	2.6	3.0	2.4	−1.4	−1.6	−0.7	−1.8	−0.9	−0.4	−1.0	−4.2	−6.6	−6.1	−6.9	−1.7
SD	1.6	1.6	3.7	2.7	0.8	2.5	1.1	1.1	1.2	1.4	1.6	2.8	1.1	0.7	1.0	1.0	1.6	1.9	2.5	2.4	1.2	3.3	1.2	1.7
−25 EX	−1.1	−2.0	0.7	−3.8	1.6	3.8	2.3	2.5	3.8	2.4	2.7	3.0	−1.4	−1.3	−0.3	−1.6	−1.4	−1.0	−0.9	−5.4	−5.8	−6.5	−7.3	−2.7
SD	1.8	1.3	2.8	2.1	0.9	2.1	0.9	1.3	0.7	1.0	1.5	2.3	0.9	0.6	0.6	0.8	0.9	1.8	2.2	1.8	1.8	2.9	1.1	1.4
−20 EX	−1.0	−2.7	−1.7	−4.7	−0.5	−3.4	1.8	1.5	3.2	2.0	1.9	3.3	−1.0	−1.0	−0.8	−1.6	−1.5	−1.5	−1.6	−6.8	−5.6	−7.4	−6.9	−3.4
SD	2.7	1.0	1.9	2.3	2.1	1.7	0.8	1.7	0.8	0.8	1.6	2.1	0.8	0.5	0.7	0.9	0.6	1.5	2.3	1.8	1.8	2.9	1.6	1.4
−10 EX	−1.6	−3.5	−2.4	−5.8	−1.0	2.6	1.5	1.8	2.9	2.1	2.2	3.3	−0.5	−0.9	−0.9	−1.6	−1.5	−1.7	−2.3	−7.5	−8.0	−5.2	−6.6	−4.1
SD	2.4	0.9	1.5	2.6	2.0	1.4	0.9	0.7	0.9	0.9	1.6	2.3	0.8	0.5	0.8	0.9	0.6	1.3	2.5	1.6	2.3	8.4	1.4	1.4
−10 EX	−3.0	−4.1	−4.3	−6.4	−0.9	1.4	2.4	1.9	2.6	2.4	2.4	4.1	−0.7	−0.5	−1.0	−1.6	−1.1	−2.3	−3.1	−7.1	−8.3	−5.3	−9.6	−4.0
SD	2.2	1.3	1.7	2.5	2.1	0.9	1.5	0.3	1.0	1.0	1.8	2.4	0.5	0.9	1.0	0.9	0.7	1.0	2.8	1.9	2.9	8.5		3.2
−0 EX		−3.9	−4.9	−6.8	0.2	1.1	2.1	2.3	2.6	2.7	1.7	4.0	−0.6	−0.5	−1.1	−1.9	−1.0	−1.3	−0.6	−3.9	−7.2	−9.0	−9.4	−4.8
SD		2.1	2.5	1.7		0.9	1.7		1.3	0.8	0.1	2.4	0.4		0.9		0.8							
0 EX																								
SD																			2.1	2.8	2.0	1.4		1.7
0 EX		−3.2	−5.2	−6.2	−1.4	1.3	2.7	2.1	2.8	2.9	1.9	4.2	−0.7	−0.4	−0.5	−1.8	−1.2	−1.3	−0.3	−2.8	−5.7	0.3	−9.1	−2.4
SD		0.7	1.6	1.3	3.7	0.9	2.0		1.2	0.7	0.4	2.4	0.3		0.7		0.7	0.6	1.8	2.1	4.8			1.6
10 EX	−4.0	−3.6	−4.5	−5.1	−0.5	2.1	3.0	2.6	3.3	3.3	3.4	3.8	−0.7	−0.1	−0.6	−1.0	−0.8	−2.7	−2.8	−6.0	−7.0	−8.8	−9.2	−2.5
SD	1.2	0.8	1.5	1.8	2.4	1.0	1.6	0.9	0.8	1.0	1.5	3.3	0.6	0.4	1.0	0.9	0.6	1.1	2.3	1.9	3.2	0.7		3.1
10 EX	−2.3	−2.6	−2.7	−3.9	0.0	−3.2	3.0	2.5	3.9	3.5	3.4	3.6	−0.2	−0.4	−0.6	−0.4	−1.4	−2.2	−1.4	−6.5	−6.6	−7.6	−6.3	−2.5
SD	1.5	1.2	1.7	1.9	2.9	1.4	1.9	1.0	0.5	1.0	1.2	3.4	1.6	0.4	1.1	0.8	0.8	1.5	2.2	1.7	2.1	0.5	1.4	3.8
20 EX	−1.5	−1.2	−1.5	−2.7	1.4	4.1	3.2	2.5	4.4	3.4	4.0	3.8	−0.9	−0.3	−0.7	−0.5	−1.3	−1.3	−0.9	−5.5	−7.9	−5.9	−6.3	−3.9
SD	1.9	1.4	1.1	2.0	3.1	1.9	1.8	1.4	0.7	0.8	1.3	3.4	0.9	0.4	1.0	0.8	0.9	2.1	2.3	1.9	0.5	1.9	1.5	1.8
20 EX	−0.8	0.3	−0.5	−2.1	3.4	4.3	3.2	3.5	4.4	3.8	4.3	3.5	−1.0	−0.2	−0.8	−0.5	−0.9	−0.1	−0.9	−5.2	−8.2	−5.7	−6.4	−3.8
SD	2.2	1.4	1.1	1.9	2.4	1.7	1.2	1.7	1.2	0.9	0.9	3.7	0.9	0.5	0.8	0.7	1.0	2.5	2.5	2.3	1.4	1.9	1.5	2.1
30 EX	−0.3	0.2	0.8	−0.3	4.7	5.0	3.4	4.0	5.0	4.6	4.2	4.0	0.1	−0.3	−0.8	−0.7	−0.5	0.3	−1.0	−5.1	−7.4	−5.8	−6.3	−3.6
SD	2.9	1.6	1.0	1.6	2.9	1.8	1.1	1.9	1.3	0.9	0.8	3.6	2.9	0.7	0.4	0.8	1.1	2.8	2.7	1.9	1.4	1.1	1.9	2.3

TABLE A2. Average Meridional Electric Fields and Standard Deviation (Equatorial Projection Part 1)

	MLT, hours																							
Altitude	0100	0200	0300	0400	0500	0600	0700	0800	0900	1000	1100	1200	1300	1400	1500	1600	1700	1800	1900	2000	2100	2200	2300	2400
1000 EX	−1.3	−1.9	−1.5	−3.2	0.2	2.6	1.8	1.5	2.7	2.2	2.3	2.5	−0.4	−0.5	−0.7	−0.8	−1.2	−1.3	−1.1	−5.0	−5.0	−5.2	−5.3	−2.7
SD	1.7	1.0	1.0	1.8	1.9	1.2	1.0	1.2	0.7	1.0	1.2	2.2	0.9	0.4	0.7	0.8	0.6	1.3	1.7	1.4	1.5	1.7	1.1	2.2
975 EX	−1.4	−1.9	−1.6	−3.3	0.1	2.6	1.8	1.5	2.8	2.2	2.3	2.5	−0.4	−0.5	−0.7	−0.8	−1.2	−1.4	−1.1	−5.0	−5.3	−5.3	−5.3	−2.7
SD	1.7	1.0	1.0	1.9	1.9	1.2	1.0	1.3	0.7	1.0	1.2	2.2	0.9	0.4	0.7	0.8	0.6	1.2	1.8	1.6	1.8	1.7	1.1	2.2
950 EX	−1.4	−2.0	−1.7	−3.3	0.1	2.5	1.8	1.5	2.8	2.3	2.3	2.6	−0.4	−0.5	−0.7	−0.8	−1.2	−1.5	−1.2	−5.1	−5.2	−5.5	−5.4	−2.8
SD	1.7	1.0	1.1	1.9	1.9	1.2	1.1	1.3	0.7	1.1	1.2	2.2	0.9	0.4	0.7	0.8	0.6	1.2	1.8	1.5	1.6	1.8	1.1	2.2
925 EX	−1.4	−2.1	−1.7	−3.4	0.0	2.5	1.8	1.5	2.8	2.3	2.4	2.6	−0.3	−0.5	−0.7	−0.8	−1.2	−1.5	1.2	−5.3	−5.3	−5.6	−5.6	−2.5
SD	1.7	1.0	1.1	1.9	1.9	1.2	1.1	1.3	0.7	1.1	1.2	2.2	1.0	0.4	0.7	0.8	0.6	1.2	1.8	1.4	1.6	1.8	1.0	2.4
900 EX	−1.5	−2.2	−1.7	−3.5	−0.1	2.5	2.0	1.5	2.8	2.3	2.4	2.6	−0.3	−0.5	−0.7	−0.9	−1.2	−1.5	−1.3	−5.3	−5.3	−6.0	−5.6	−2.4
SD	1.7	1.0	1.1	1.9	2.0	1.2	1.3	1.3	0.7	1.1	1.2	2.2	1.0	0.4	0.7	0.8	0.6	1.2	1.8	1.5	1.7	1.8	1.0	2.6
875 EX	−1.5	−2.2	−1.8	−3.6	−0.1	2.4	2.0	1.8	2.8	2.4	2.4	2.6	−0.3	−0.5	−0.7	−0.8	−1.2	−1.5	−1.3	−5.4	−5.4	−6.0	−5.7	−2.4
SD	1.7	1.0	1.2	1.9	2.0	1.1	1.3	0.8	0.7	1.1	1.2	2.2	1.0	0.4	0.7	0.8	0.6	1.2	1.9	1.5	1.7	1.8	1.0	2.6
850 EX	−1.6	−2.3	−1.9	−3.7	−0.2	2.4	2.0	1.8	2.8	2.4	2.4	2.7	−0.3	−0.5	−0.6	−0.8	−1.3	−1.6	−1.4	−5.6	−5.4	−6.1	−5.7	−2.5
SD	1.7	0.9	1.2	2.0	2.0	1.2	1.4	0.8	0.7	1.1	1.2	2.3	1.0	0.4	0.8	0.8	0.6	1.2	1.9	1.4	1.8	1.9	1.0	2.6
825 EX	−1.6	−2.4	−1.9	−3.8	−0.3	2.4	1.9	1.8	2.8	2.4	2.4	2.7	−0.3	−0.6	−0.6	−0.8	−1.3	−1.6	−1.4	−5.7	−5.4	−6.4	−5.7	−2.4
SD	1.7	0.9	1.2	2.0	2.0	1.2	1.4	0.7	0.7	1.1	1.2	2.3	1.0	0.4	0.8	0.8	0.6	1.2	1.9	1.4	1.8	1.6	1.0	2.8
800 EX	−1.7	−2.5	−2.0	−3.9	−0.3	2.4	1.9	1.9	2.7	2.4	2.4	2.7	−0.3	−0.6	−0.6	−0.8	−1.3	−1.7	−1.5	−5.8	−5.5	−6.9	−5.8	−2.4
SD	1.7	1.0	1.2	2.0	2.0	1.1	1.4	0.7	0.7	1.1	1.2	2.3	1.0	0.4	0.8	0.9	0.6	1.2	1.9	1.5	1.8	1.0	1.0	2.8
775 EX	−1.7	−2.6	−2.1	−4.0	−0.4	2.3	1.9	1.9	2.7	2.4	2.4	2.9	−0.3	−0.6	−0.6	−0.8	−1.3	−1.7	−1.5	−5.9	−5.7	−7.0	−5.7	−2.9
SD	1.7	1.0	1.2	2.0	2.1	1.1	1.4	0.7	0.7	1.1	1.2	2.3	1.0	0.4	0.8	0.8	0.7	1.2	1.9	1.4	1.9	1.0	1.5	2.5
750 EX	−1.9	−2.6	2.2	−4.1	−0.5	2.2	1.9	2.0	2.8	2.4	2.4	2.9	−0.3	−0.6	−0.6	−0.9	−1.3	−1.8	−1.6	−6.1	−5.8	−7.1	−5.8	−3.1
SD	1.8	0.9	1.2	2.0	2.1	1.1	1.4	0.6	0.7	1.1	1.2	2.3	1.0	0.4	0.8	0.9	0.7	1.1	2.0	1.6	2.2	1.0	1.5	2.4
725 EX	−1.9	−2.7	−2.4	−4.2	−0.6	2.2	1.9	2.0	2.8	2.5	2.4	2.9	−0.3	−0.6	−0.9	−0.9	−1.8	−1.8	−1.7	−6.1	−5.8	−7.2	−5.9	−3.1
SD	1.8	0.9	1.1	2.1	2.1	1.0	1.4	0.6	0.7	1.1	1.2	2.3	1.0	0.4	0.9	0.8	0.6	1.1	2.0	1.5	2.1	1.0	1.5	2.4
700 EX	−1.9	−2.9	−2.7	−4.3	−0.7	2.2	1.8	2.0	2.8	2.4	2.4	3.0	−0.3	−0.6	−0.6	−0.9	−1.2	−1.9	−1.7	−6.2	−5.8	−7.3	−5.9	−3.1
SD	1.7	0.8	1.0	2.1	2.1	1.0	1.4	0.6	0.7	1.1	1.2	2.3	1.0	0.4	0.9	0.8	0.7	1.1	2.1	1.5	2.0	1.0	1.5	2.3
675 EX	−2.2	−2.9	−3.0	−4.4	−0.7	2.1	1.8	2.0	2.8	2.5	2.4	3.0	−0.3	0.6	−0.6	−0.9	−1.2	−1.9	−1.8	−6.2	−5.9	−7.5	−5.1	−3.4
SD	2.1	0.9	0.9	2.1	2.2	1.0	1.5	0.6	0.7	1.1	1.2	2.3	1.1	0.4	0.9	0.8	0.6	1.1	2.1	1.6	2.1	1.0	1.5	2.5
650 EX	−2.2	−3.0	−3.1	−4.6	−0.8	2.1	1.8	2.0	2.8	2.5	2.5	3.4	−0.3	−0.6	−0.6	−1.0	−1.3	−2.0	−1.9	−6.4	−5.9	−7.5	−6.2	−3.5
SD	2.5	0.9	0.9	2.1	2.2	1.0	1.5	0.6	0.7	1.1	1.2	2.1	1.1	0.5	0.9	0.8	0.7	1.1	2.1	1.6	2.2	1.0	1.5	2.5

TABLE A4. Average Zonal Ion Flow and Standard Deviation (300-km Projection)

		MLT, hours																						
Latitude		0100	0200	0300	0400	0500	0600	0700	0800	0900	1000	1100	1200	1300	1400	1500	1600	1700	1800	1900	2000	2100	2200	2300	2400
−30	VEL	36.	−44.	11.	139.	92.	−117.	−100.	−77.	−115.	−74.	−92.	−63.	43.	59.	18.	50.	29.	5.	30.	110.	252.	176.	222.	60.
	SD	56.5	57.	91.1	92.2	35.4	50.5	27.5	45.3	18.4	34.9	47.8	77.5	31.9	31.6	28.4	23.0	40.7	56.9	80.3	68.1	61.5	51.5	47.5	63.9
−25	VEL	43.	−57.	−18.	122.	−67.	−111.	−80.	−75.	−101.	−73.	−82.	−89.	46.	47.	11.	46.	42.	26.	29.	153.	227.	180.	230.	89.
	SD	64.8	50.5	79.2	79.2	38.5	49.5	30.3	38.5	13.4	30.2	31.7	67.2	30.1	25.9	21.0	21.3	23.3	51.6	72.9	60.5	83.2	48.3	48.9	61.7
−20	VEL	42.	96.	65.	158.	6.	−98.	−64.	−45.	−94.	−66.	−61.	−102.	35.	38.	32.	45.	47.	44.	51.	198.	223.	209.	229.	106.
	SD	83.8	42.3	75.7	83.2	64.2	43.2	29.6	61.1	17.6	28.1	38.9	60.9	27.5	23.4	29.6	22.1	20.2	42.1	72.9	50.0	82.7	46.5	61.2	54.4
−15	VEL	61.	120.	82.	195.	29.	−77.	−56.	−65.	−89.	−69.	−73.	−108.	21.	33.	37.	47.	51.	56.	76.	226.	316.	149.	225.	121.
	SD	80.0	33.0	55.3	90.5	66.1	35.2	33.5	27.6	23.0	26.4	40.5	73.2	27.6	20.2	32.8	24.8	24.9	35.6	83.1	44.9	43.8	225.9	37.9	42.6
−10	VEL	109.	139.	144.	223.	31.	−46	−81.	−74.	−84.	−76.	−78.	−137.	−26.	−21.	39.	49.	−33.	−82.	105.	219.	340.	161.	263.	125.
	SD	76.5	44.5	41.9	85.8	71.1	25.9	37.0	24.6	32.0	28.3	45.9	75.9	22.7	35.8	44.1	27.5	22.0	24.1	89.3	47.9	48.32	242.7		100.1
−5	VEL		138.	164.	242.	−8.	−38.	−67.	−107.	−83.	−90.	−60.	−137.	23.	22.	39.	54.	34.	42.	19.	117.	296.	289.	267.	156.
	SD		75.2	60.2	50.8		28.9	44.0		44.8	25.7	1.4	77.3	12.6		30.9		24.1		70.8	83.0	57.4	7.9		53.9
0	VEL																								
	SD																								
5	VEL		106.	174.	212.	48.	−42.	−78.	−89.	−90.	96.	−63.	−139.	24.	16.	19.	50.	41.	41.	8.	86.	203.	−7.	262.	112.
	SD		35.2	48.9	33.8	128.3	27.1	51.2		42.6	23.7	13.7	75.9	11.4		22.1		23.5	14.8	63.3	61.1	157.4			55.0
10	VEL	141.	116.	144.	170.	15.	−65.	−89.	−87.	−104.	−101.	−106.	−119.	23.	4.	23.	30.	27.	88.	89.	184.	240.	249.	257.	82.
	SD	25.5	32.2	45.6	59.1	79.7	23.1	37.9	12.6	27.8	23.5	44.6	102.5	23.7	14.0	36.3	24.1	19.6	31.6	69.7	47.9	87.5	20.5		102.0
15	VEL	75.	81.	84.	124.	−3.	−95.	−88.	−78.	−116.	−105.	−104.	−105.	11.	12.	20.	11.	43.	71.	43.	190.	215.	205.	202.	79.
	SD	51.5	39.5	55.1	65.4	92.1	30.9	46.0	29.3	13.3	20.8	33.9	98.8	44.0	12.1	36.6	21.1	24.3	44.2	65.3	39.8	55.5	10.8	35.3	116.5
20	VEL	50.	36.	44.	80.	−47.	−117.	−88.	−74.	−123.	−102.	−114.	−106.	27.	10.	22.	13.	39.	36.	23.	150.	233.	158.	192.	122.
	SD	60.7	43.1	33.2	66.4	97.1	41.0	38.3	44.5	11.5	16.7	29.2	94.3	28.6	13.0	29.6	22.3	28.2	61.0	66.0	47.1	24.3	41.3	41.5	53.0
25	VEL	26.	−8.	14.	60.	−106.	−122.	−84.	−98.	−111.	−110.	−118.	−94.	29.	6.	23.	13.	26.	2.	22.	136.	223.	144.	186.	109.
	SD	62.0	38.9	34.3	56.3	72.9	46.3	21.9	48.9	22.3	25.4	25.2	100.1	29.0	14.3	22.2	16.6	29.0	72.6	68.9	56.6	2.3	38.5	42.8	57.3
30	VEL	13.	−32.	−21.	12.	−130.	−133.	−91.	−105.	−125.	−117.	−107.	−100.	−1.	8.	22.	15.	14.	−13.	22.	123.	189.	145.	172.	99.
	SD	75.3	44.7	26.9	43.9	81.6	51.4	21.5	50.5	25.9	22.5	22.4	93.4	75.0	19.5	12.0	18.2	29.7	73.6	70.0	43.2	24.3	34.8	51.7	63.4

TABLE A3. Average Meridional Electric Fields and Standard Deviation (Equatorial Projection Part 2)

	SD																							
	1.7	0.8	0.9	2.1	2.3	1.0	1.4	0.6	0.7	1.1	1.3	2.2	1.1	0.4	0.9	0.8	0.7	1.1	2.2	1.6	2.3	1.0	1.8	2.8
600 EX	−2.9	−3.3	−3.3	−4.8	−0.7	1.9	1.8	1.9	2.8	2.5	2.7	3.7	−0.2	−0.6	−0.7	−1.1	−1.2	−2.1	−2.2	−6.4	−6.1	−7.7	−6.2	−3.2
SD	1.6	0.8	1.0	2.1	2.1	1.0	1.4	0.6	0.8	1.1	1.5	2.4	1.1	0.4	0.9	0.8	0.8	1.0	2.2	1.7	2.3	0.9	2.0	2.8
575 EX	−3.0	−3.4	−3.5	−5.0	−0.8	1.9	1.7	1.9	2.8	2.6	2.6	3.5	−0.2	−0.6	−0.7	−1.1	−1.2	−2.1	−2.4	−6.4	−6.2	−7.9	−6.1	−3.1
SD	1.6	0.8	1.3	2.1	2.1	1.0	1.4	0.6	0.8	1.1	1.5	2.5	1.1	0.5	0.9	0.8	0.8	1.0	2.2	2.0	2.3	0.9	3.4	2.9
550 EX	−3.0	−3.5	−3.6	−5.1	−0.5	1.7	1.9	1.9	2.8	2.6	2.7	3.6	−0.2	−0.5	−0.7	−1.1	−1.2	−2.2	−2.5	−6.5	−6.2	−8.0	−6.3	−3.1
SD	1.5	0.8	1.3	2.0	2.0	0.9	1.5	0.6	0.9	1.1	1.5	2.5	1.1	0.6	0.9	0.9	0.8	1.0	2.3	1.8	2.6	0.9	4.9	2.9
525 EX	−3.1	−3.5	−3.8	−5.2	−0.6	1.7	2.4	1.9	2.7	2.6	2.8	3.6	−0.2	−0.3	−0.7	−1.2	−0.9	−2.3	−2.7	−6.4	−6.2	−8.2	−6.4	−3.2
SD	1.5	1.0	1.4	2.0	2.0	0.8	1.2	0.6	0.8	1.1	1.5	2.5	1.1	0.7	0.9	0.9	0.5	0.9	2.3	1.8	2.7	0.9	5.0	2.8
500 EX	−3.1	−3.4	−4.0	−5.8	−0.7	1.6	2.5	2.1	2.7	2.7	2.7	3.6	−0.6	−0.2	−0.7	−1.3	−0.9	−2.1	−2.8	−6.2	−6.4	−8.3	−6.5	−3.3
SD	1.5	1.0	1.4	1.5	2.0	0.9	1.3	0.6	0.9	1.1	1.5	2.6	0.5	0.7	0.9	0.9	0.6	0.8	2.3	1.8	3.1	0.9	5.1	2.9
475 EX	−3.1	−3.5	−4.1	−5.9	−0.7	1.5	2.4	2.1	2.7	2.7	2.7	3.7	−0.8	0.4	−0.8	−1.2	−1.1	−2.1	−2.7	−5.8	−6.5	−8.5	−6.6	−3.3
SD	1.4	1.0	1.5	1.5	2.1	0.9	1.3	0.6	0.9	1.1	1.7	2.6	0.4	0.6	0.9	0.9	0.6	0.8	2.3	2.0	2.9	0.9	5.1	2.9
450 EX	−3.0	−3.6	−4.3	−6.0	−0.7	1.4	2.5	2.0	2.7	2.7	3.1	3.7	−0.8	−0.7	−0.8	−1.3	−1.1	−1.9	−2.7	−5.2	−6.5	−6.6	−6.6	−3.5
SD	0.6	1.1	1.5	1.5	2.2	0.9	1.3	0.5	0.9	1.0	1.9	2.5	0.4	0.7	0.9	1.0	0.6	0.6	2.3	2.2	3.2	5.9	5.1	2.9
425 EX	−3.0	−3.3	−4.4	−6.1	−0.9	1.3	2.6	2.4	2.6	2.7	3.2	3.7	−0.7	−0.6	−0.8	−1.2	−1.2	−1.8	−2.5	−4.6	−6.6	−8.7	−6.7	−3.4
SD	0.5	1.3	1.6	1.4	2.3	0.9	1.6	0.5	0.9	1.0	2.1	2.5	0.4	0.7	1.0	0.9	0.6	0.6	2.2	2.6	3.3	1.0	5.2	2.9
400 EX	−3.1	−3.3	−4.5	−6.1	−0.8	1.2	2.5	2.4	2.6	2.9	3.2	3.9	−0.7	−0.6	−0.8	−1.2	−1.2	−1.7	−2.1	−4.1	−5.1	−8.4	−6.7	−3.5
SD	0.4	1.4	1.7	1.4	2.3	0.8	1.6	0.4	1.0	1.0	2.1	2.3	0.4	0.6	0.7	0.8	0.6	0.6	2.0	2.8	2.4	0.8	5.2	2.9
375 EX	−3.0	−3.4	−4.7	−6.1	−0.4	1.1	2.4	2.2	2.5	2.9	1.8	4.0	−0.7	−0.8	−0.7	−1.8	−1.1	−1.6	−1.3	−3.6	−5.5	−8.5	−6.7	−3.9
SD	0.6	1.4	1.8	1.4	2.6	0.8	1.6	0.1	1.1	1.0	0.3	2.2	0.3	0.4	0.7	0.5	0.6	0.6	1.9	2.5	2.4	0.8	5.2	2.5
350 EX	−3.1	−3.3	−4.7	−6.2	−0.5	1.1	2.3	2.1	2.5	2.8	1.7	3.9	−0.6	−0.4	−0.8		−1.1	−1.2	−0.4	−3.0	−5.0	−8.0	−6.7	−4.4
SD	0.7	1.5	1.8	1.5	3.2	0.9	1.6	0.1	1.2	0.9	0.2	2.2	0.3	0.0	0.7		0.6	0.4	1.8	2.3	3.4	1.2	5.2	1.6
325 EX	−3.0	−3.3	−4.7	−5.9		0.9	2.7	2.0	2.6	2.7	1.8	4.2		−0.5	0.8		−1.1	−1.1	0.5	−2.1	−3.3	−9.1		−4.3
SD	0.7	1.5	1.8	1.5		0.6	1.6	0.0	1.2	0.9	0.3	2.0		0.0	0.8		0.3	0.3	1.9	1.7	3.4	0.4		1.6
300 EX	−2.9	−2.7	−4.9	−3.0		0.9			2.6	4.0					0.9			0.9	0.1					−4.3
SD	0.4	0.6	1.8	0.5		0.6			1.3	0.1					0.9			0.3	1.1					1.8
275 EX		−2.6	−4.9	−2.8																				
SD		0.8	2.0	0.1																				

electric fields perpendicular to the magnetic field versus magnetic latitude for the 300-km projection. Tables A2 and A3 display the vertical electric field versus altitude at the magnetic equator for the projection to the equatorial plane. Table A4 lists the average zonal ion drift velocities derived from the electric field data versus latitude for the 300-km projection.

Each table also presents values for the standard deviation of the data set for each point. The sample size at each point in the 300-km projection is given in Table 1. Since the data set is so small at the equator because of orbit coverage (see main text), no equatorial samples are included. The coverage for the equatorial projection is similar, with the higher altitudes corresponding to the higher latitudes and the lower altitudes corresponding to the lower latitudes. Where the standard deviation is omitted in the tables represents data sets of only one value.

Acknowledgments. The Editor thanks J. H. A. Sobral and another referee for their assistance in evaluating this paper.

REFERENCES

Abdu, M. A., I. J. Kantor, I. S. Batista, and E. R. Paula, East-west plasma bubble irregularity motion determined from spaced VHF polarimeters: Implications on velocity shear in the zonal *F* region bulk plasma motion, *Radio Sci., 20*, 111, 1985.

Aggson, T. L., N. C. Maynard, F. A. Herrero, H. G. Mayr, L. H. Brace, and M. C. Liebrecht, Geomagnetic equatorial anomaly in zonal plasma flow, *J. Geophys. Res., 92*, 311, 1987.

Anderson, D. N., and M. Mendillo, Ionospheric conditions affecting the evolution of equatorial plasma depletions, *Geophys. Res. Lett., 10*, 541, 1983.

Basu, S., J. P. McClure, S. Basu, W. B. Hanson, and J. Aarons, Coordinated study of equatorial scintillation and in situ and radar observations of nighttime *F* region irregularities, *J. Geophys. Res., 85*, 5119, 1980.

Behnke, R. A., and R. M. Harper, Vector measurements of *F* region ion transport at Arecibo, *J. Geophys. Res., 78*, 8222, 1973.

Blanc, M., and P. Amayenc, Seasonal variations of the ionospheric **E** × **B** drifts above Saint-Santin on quiet days, *J. Geophys. Res., 84*, 2691, 1979.

Blanc, M., and A. D. Richmond, The ionospheric disturbance dynamo, *J. Geophys. Res., 85*, 1669, 1980.

Dickinson, R. E., E. C. Ridley, and R. G. Roble, Meridional circulation in the thermosphere, I, Equinox conditions, *J. Atmos. Sci., 32*, 1737, 1975.

Dickinson, R. E., E. C. Ridley, and R. G. Roble, Meridional circulation in the thermosphere, I, Equinox conditions, *J. Atmos. Sci., 34*, 178, 1977.

Fejer, B. G., The equatorial ionospheric electric fields: A review, *J. Atmos. Terr. Phys., 43*, 377, 1981.

Fejer, B. G., D. T. Farley, C. A. Gonzales, R. F. Woodman, and C. Calderon, *F* region east-west drifts at Jicamarca, *J. Geophys. Res., 86*, 215, 1981.

Fejer, B. G., E. Kudecki, and D. J. Farley, Equatorial *F* region zonal plasma drift, *J. Geophys. Res., 90*, 12,249, 1985.

Forbes, J. M., and D. F. Gillette, A compendium of theoretical atmospheric tidal structures, *Rep. AFGL-TR-82-0173(I)*, Air Force Geophys. Lab., Hanscom Air Force Base, Mass., 1982.

Ganguly, S., R. A. Behnke, and B. A. Emery, Average electric field behavior in the ionosphere above Arecibo, *J. Geophys. Res., 92*, 1199, 1987.

Heelis, R. A., P. C. Kendall, R. J. Moffet, D. W. Windle, and H. Rishbeth, Electrical coupling of the *E* and *F* regions and its effect on *F* region drifts and winds, *Planet. Space Sci., 21*, 743, 1974.

Herrero, F. A., and H. G. Mayr, Tidal decompositions of zonal neutral and ion flows in the Earth's upper equatorial thermosphere, *Geophys. Res. Lett., 13*, 359, 1986.

Herrero, F. A., H. G. Mayr, and N. W. Spencer, Latitudinal (seasonal) variations in the thermospheric midnight temperature maximum: A tidal analysis, *J. Geophys. Res., 88*, 7225, 1983.

Krehbiel, J. P., L. H. Brace, R. F. Theis, W. H. Pinkus, and R. B. Kaplan, The Dynamics Explorer Langmuir probe instrument, *Space Sci. Instrum., 5*, 493, 1981.

Kudeki, E., B. G. Fejer, D. T. Farley, and H. M. Ierkic, Interferometer studies of equatorial *F* region irregularities and drifts, *Geophys. Res. Lett., 8*, 377, 1981.

Maynard, N. C., E. A. Bielecki, and H. F. Burdick, Instrumentation for vector electric field measurements from DE B, *Space Sci. Instrum., 5*, 523, 1981.

Maynard, N. C., J. P. Heppner, and A. Egeland, Intense, variable electric fields at ionospheric altitudes in the high-latitude regions as observed by DE 2, *Geophys. Res. Lett., 9*, 981, 1982.

Richmond, A. D., S. Mitsushita, and J. D. Tarpley, On the production mechanisms of electric currents and fields in the ionosphere, *J. Geophys. Res., 81*, 547, 1976.

Richmond, A. D., M. Blanc, B. A. Emery, R. H. Wand, B. G. Fejer, R. F. Woodman, S. Ganguly, P. Amayenc, R. A. Behnke, C. Calderon, and J. V. Evans, An empirical model of quiet-ionospheric electric fields at middle and low latitudes, *J. Geophys. Res., 85*, 4658, 1980.

Rishbeth, H., The *F*-region dynamo, *Planet. Space Sci., 19*, 263, 1971.

Takeda, M., and H. Maeda, *F*-region dynamo in the evening—Interpretation of equatorial ΔD anomaly found by MAGSAT, *J. Atmos. Terr. Phys., 45*, 401, 1983.

Wharton, L. E., N. W. Spencer, and H. C. Mayr, The Earth's thermospheric superrotation from Dynamics Explorer 2, *Geophys. Res. Lett., 11*, 531, 1984.

Woodman, R. F., East-west ionospheric drifts at the magnetic equator, *Space Res., 12*, 969, 1972.

T. L. Aggson and F. A. Herrero, NASA Goddard Space Flight Center, Greenbelt, MD 20771.

M. C. Liebrecht, Science Applications Research Inc., Lanham, MD 20706.

N. C. Maynard, Air Force Geophysics Laboratory, Hanscom Air Force Base, MA 01731.

(Received July 28, 1987;
revised December 1, 1987;
accepted December 2, 1987.)